

1 Cryo-EM structures of  $\alpha$ -synuclein filaments from  
2 Parkinson's disease and dementia with Lewy  
3 bodies

4

5

6 Yang Yang<sup>1</sup>, Yang Shi<sup>1</sup>, Manuel Schweighauser<sup>1</sup>, Xianjun Zhang<sup>2</sup>, Abhay  
7 Kotecha<sup>2</sup>, Alexey G. Murzin<sup>1</sup>, Holly J. Garringer<sup>3</sup>, Patrick W. Cullinane<sup>4,5</sup>,  
8 Yuko Saito<sup>6</sup>, Tatiana Foroud<sup>7</sup>, Thomas T. Warner<sup>4,5</sup>, Kazuko Hasegawa<sup>8</sup>,  
9 Ruben Vidal<sup>3</sup>, Shigeo Murayama<sup>9</sup>, Tamas Revesz<sup>5,10</sup>, Bernardino Ghetti<sup>3</sup>,  
10 Masato Hasegawa<sup>11</sup>, Tammaryn Lashley<sup>5,10</sup>, Sjors H.W. Scheres<sup>1,12</sup>, Michel  
11 Goedert<sup>1,12</sup>

12

13

14

15 <sup>1</sup> Medical Research Council Laboratory of Molecular Biology, Cambridge, UK

16 <sup>2</sup> Thermo Fisher Scientific, Eindhoven, The Netherlands

17 <sup>3</sup> Department of Pathology and Laboratory Medicine, Indiana University  
18 School of Medicine, Indianapolis, IN, USA

19 <sup>4</sup> Department of Clinical and Movement Neurosciences, Queen Square  
20 Institute of Neurology, University College London, UK

21 <sup>5</sup> Queen Square Brain Bank for Neurological Disorders, Institute of  
22 Neurology, University College London, UK

23 <sup>6</sup> Department of Neuropathology, Metropolitan Institute of Gerontology,  
24 Tokyo, Japan

25 <sup>7</sup> Department of Medical and Molecular Genetics, Indiana University School  
26 of Medicine, Indianapolis, IN, USA

27 <sup>8</sup> Division of Neurology, Sagamihara National Hospital, Sagamihara, Japan

28 <sup>9</sup> Molecular Research Centre for Children's Mental Development, United  
29 School of Child Development, University of Osaka, Osaka, Japan

30 <sup>10</sup> Department of Neurodegenerative Disease, Queen Square Institute of  
31 Neurology, University College London, UK

32 <sup>11</sup> Department of Brain and Neurosciences, Metropolitan Institute of Medical  
33 Science, Tokyo, Japan

34

35 <sup>12</sup> These authors jointly supervised this work: Sjors H.W. Scheres, Michel  
36 Goedert. E-mail: [scheres@mrc-lmb.cam.ac.uk](mailto:scheres@mrc-lmb.cam.ac.uk); [mg@mrc-lmb.cam.ac.uk](mailto:mg@mrc-lmb.cam.ac.uk)

37

38

39

40

41 Parkinson's disease (PD) is the most common movement disorder,  
42 with resting tremor, rigidity, bradykinesia and postural instability  
43 being major symptoms (1). Neuropathologically, it is characterised  
44 by the presence of abundant filamentous inclusions of  $\alpha$ -synuclein  
45 in the form of Lewy bodies and Lewy neurites in some brain cells,  
46 including dopaminergic nerve cells of the substantia nigra (2). PD  
47 is increasingly recognised as a multisystem disorder, with cognitive  
48 decline being one of its most common non-motor symptoms. Many  
49 patients with PD develop dementia more than 10 years after  
50 diagnosis (3). PD dementia (PDD) is clinically and  
51 neuropathologically similar to dementia with Lewy bodies (DLB),  
52 which is diagnosed when cognitive impairment precedes  
53 parkinsonian motor signs or begins within one year from their  
54 onset (4). In PDD, cognitive impairment develops in the setting of  
55 well-established PD. Besides PD and DLB, multiple system atrophy  
56 (MSA) is the third major synucleinopathy (5). It is characterised by  
57 the presence of abundant filamentous  $\alpha$ -synuclein inclusions in  
58 brain cells, especially oligodendrocytes (Papp-Lantos bodies). We  
59 previously reported the electron cryo-microscopy (cryo-EM)  
60 structures of two types of  $\alpha$ -synuclein filaments extracted from the  
61 brains of individuals with MSA (6). Each filament type is made of  
62 two different protofilaments. Here we report that the cryo-EM  
63 structures of  $\alpha$ -synuclein filaments from the brains of individuals  
64 with PD, PDD and DLB are made of a single protofilament (Lewy  
65 fold) that is markedly different from the protofilaments of MSA.  
66 These findings establish the existence of distinct molecular  
67 conformers of assembled  $\alpha$ -synuclein in neurodegenerative  
68 disease.

69  
70 A causal link between  $\alpha$ -synuclein assembly and disease was established  
71 by the findings that missense mutations in *SNCA* (the gene that encodes  
72  $\alpha$ -synuclein) and multiplications (duplications and triplications) of this gene  
73 give rise to inherited forms of PD and PDD (7,8). Some mutations also  
74 cause DLB (8,9). Sequence variation in the regulatory region of *SNCA* is  
75 associated with increased expression of  $\alpha$ -synuclein and a heightened risk  
76 of developing idiopathic PD, which accounts for over 90% of cases of  
77 disease (10). Both inherited and idiopathic cases of PD, PDD and DLB are  
78 characterised by the presence of abundant Lewy bodies and Lewy neurites  
79 in central and peripheral nervous systems (2).

80

81         $\alpha$ -Synuclein is a 140-amino acid protein, over half of which (residues 7-  
82        87) consists of seven imperfect repeats, which are lipid-binding domains  
83        (11). They partially overlap with a hydrophobic region (residues 61-95),  
84        also known as the non- $\beta$ -amyloid component (NAC) (12), which is  
85        necessary for the assembly of recombinant  $\alpha$ -synuclein into filaments (13).  
86        The carboxy-terminal region (residues 96-140) is negatively charged and  
87        its truncation results in increased filament formation (14). Upon assembly,  
88        recombinant  $\alpha$ -synuclein undergoes conformational changes and takes on  
89        a cross- $\beta$  structure that is characteristic of amyloid (15,16). The core of  $\alpha$ -  
90        synuclein filaments assembled from recombinant protein *in vitro* extends  
91        from approximately residues 30-100 (17).

92  
93        Seeded assembly of  $\alpha$ -synuclein, propagation of inclusions and nerve cell  
94        death have been demonstrated in a variety of systems (18-21). Assemblies  
95        of  $\alpha$ -synuclein with different morphologies display distinct seeding  
96        capacities (22,23). Indirect evidence has also suggested that different  
97        conformers of assembled  $\alpha$ -synuclein may characterise disorders with Lewy  
98        pathology and MSA (24-31).

99

100

101        Neuropathological characteristics and filament characterisation

102

103        We used sarkosyl to extract filaments from the cingulate cortex of an  
104        individual with a neuropathologically confirmed diagnosis of PD, two  
105        individuals with PDD and one individual with DLB (case 3). Frontal cortex  
106        was used for DLB cases 1 and 2. The individual with PD had a disease  
107        duration of 22 years and an age at death of 78 years; the individuals with  
108        PDD had disease durations of 8 and 13 years and ages at death of 87 and  
109        76 years, respectively; DLB case 1 was in a 59-year-old individual with a  
110        disease duration of 10 years; DLB case 2 was in a 74-year-old individual  
111        with a disease duration of 13 years; DLB case 3 was in a 78-year-old  
112        individual with a disease duration of 15 years. Abundant Lewy bodies and  
113        Lewy neurites were stained by antibody Syn1, which is specific for the NAC  
114        region of  $\alpha$ -synuclein (Extended Data Figure 1). Some glial cell staining  
115        was also present in DLB case 3. By negative-stain electron microscopy,  
116        cases of PD, PDD and DLB showed filaments with a diameter of 10 nm.  
117        Immunogold negative-stain electron microscopy with anti- $\alpha$ -synuclein  
118        antibody PER4 showed decoration of filaments, consistent with previous  
119        findings (Extended Data Figure 2a-c) (6,32,33). Immunoblotting of  
120        sarkosyl-insoluble material from the cases of PD, PDD and DLB with  
121        antibodies Syn303, Syn1 and PER4 showed high-molecular weight material

122 (Extended Data Figure 2d-f). Full-length  $\alpha$ -synuclein was the  
123 predominant species in most cases, but truncated  $\alpha$ -synuclein was also  
124 present. The sequences of the coding exons of *SNCA* were wild-type in PD,  
125 PDD1, PDD2, DLB1, DLB2 and DLB3. We used cryo-EM to determine the  
126 atomic structures of  $\alpha$ -synuclein filaments from all six cases (Figure 1;  
127 Methods; Extended Data Figures 3 and 4; Extended Data Tables 1  
128 and 2).

129

130

### 131 $\alpha$ -Synuclein filaments of PD, PDD and DLB

132

133 In agreement with previous observations for DLB (6), most filaments  
134 from the cases with PD, PDD and DLB did not exhibit a helical twist in the  
135 cryo-EM micrographs. Still, for each case, a minority of filaments (~25%)  
136 was twisted, allowing their structure determination by helical  
137 reconstruction.  $\alpha$ -Synuclein filaments from PD, PDD and DLB are identical  
138 and comprise a single protofilament (Figures 1 and 2). We termed the  
139 structure of the ordered core of these filaments "Lewy fold". The  
140 reconstruction with the highest resolution, 2.2 Å for case 1 of PDD, showed  
141 density for main-chain oxygen atoms (Extended Data Figure 3c),  
142 establishing that  $\alpha$ -synuclein filaments with the Lewy fold have a right-  
143 handed twist, in contrast to the left-handed twist observed for  $\alpha$ -synuclein  
144 filaments with the MSA fold (6).

145

146 We did not determine the structures of the untwisted filaments.  
147 Nevertheless, most 2D class averages of untwisted filaments resembled  
148 projections of untwisted filament models with the Lewy fold (Extended  
149 Data Figure 4a-h). Moreover, stretches of segments that gave rise to  
150 twisted 2D class averages were typically observed together with stretches  
151 of segments giving rise to untwisted 2D class averages within the same  
152 filaments (Extended Data Figure 4i-k). It is thus likely that most of the  
153 untwisted filaments also adopted the Lewy fold, although we cannot  
154 exclude the presence of additional, minority folds among untwisted  
155 filaments. It is possible that cryo-EM grid preparation leads to untwisting  
156 of filaments, and it remains to be investigated whether filaments with a  
157 right-handed twist are more prone to untwisting than those with a left-  
158 handed twist.

159

160 The Lewy fold is formed by residues 31-100 of  $\alpha$ -synuclein, which  
161 arrange as nine  $\beta$ -strands ( $\beta$ 1-9) in a three-layered structure (Figure 2).  
162 The first two layers are corrugated, with the first comprising  $\beta$ 1-5 and the

163 second  $\beta$ 6-8. The third layer consists only of  $\beta$ 9. Two additional, partial  
164 layers are made by densities (islands) that are not connected to the rest of  
165 the ordered core. Island A packs against  $\beta$ 5; island B packs against the N-  
166 terminal half of  $\beta$ 9. The reconstructed densities for both islands indicate  
167 that they are made of peptides, but a lack of distinct side chain densities  
168 precluded their identification.

169

170 Besides the density for the ordered core of  $\alpha$ -synuclein filaments and  
171 islands A and B, there are several additional densities in the cryo-EM  
172 reconstruction that could not be explained by peptides. We observed a  
173 density that is approximately 55  $\text{\AA}^3$  in size, in front of K32, K34, Y39, K43  
174 and K45 (Figure 3). Its size and chemical environment resemble those of  
175 the unidentified cofactors in the  $\alpha$ -synuclein filaments from MSA. Its  
176 position, in the middle of an outside groove formed by  $\beta$ 1-3, suggests that  
177 the corresponding cofactors may be important for formation of the Lewy  
178 fold. Smaller, spherical densities next to Y39 and T44 probably  
179 corresponded to solvent molecules.

180

181 The Lewy fold differs from the structures of MSA filaments from human  
182 brains (6) and from those of *in vitro* assembled  $\alpha$ -synuclein filaments (34).  
183 Whereas Lewy and MSA folds are different, substructures of the Lewy fold  
184 have been observed in  $\alpha$ -synuclein filaments that were assembled *in vitro*  
185 (Figure 3; Extended Data Figure 5). Residues 32-41 and 70-82 overlay  
186 with a root-mean-square deviation of the main-chain atoms (rmsd) of 1.1  
187  $\text{\AA}$  with the same residues in a recombinant  $\alpha$ -synuclein filament with  
188 phosphorylation of Y39 (35) (PDB:6L1T). Residues 42-67 also overlay with  
189 a rmsd of 1.3  $\text{\AA}$  onto the same structure, albeit in a different orientation  
190 relative to the rest of the fold. Both substructures contribute to the  
191 electrostatic interaction network around the phosphate group of Y39.  
192 However, in the Lewy fold, there is no additional density at Y39, indicating  
193 that this residue is not phosphorylated. Instead, both substructures form  
194 the cofactor-binding groove. In the “hinge” region, between residues 42-  
195 67 and 70-82, residues 61-72 adopt essentially the same conformation as  
196 in the  $\alpha$ -synuclein filaments from MSA and some filaments assembled from  
197 recombinant proteins. In addition, residues 69-98 of the Lewy fold overlay  
198 with a rmsd of 0.5  $\text{\AA}$  with the same residues in filaments of N-terminally  
199 truncated recombinant  $\alpha$ -synuclein (41-140) (36) (PDB:7LC9).  
200 Interestingly, residues 85-92, as well as the peptide corresponding to the  
201 density of island A, overlay with a rmsd of 0.5  $\text{\AA}$  with residues 14-23 and  
202 85-92 of recombinant  $\alpha$ -synuclein filament polymorph 2a that was  
203 assembled from full-length recombinant protein (36) (PDB:6SSX). In this

204 structure, the density for residues 14-23 is also disconnected from the rest  
205 of the ordered core. It is therefore likely that the peptide corresponding to  
206 island A in the Lewy fold corresponds to part of the  $\alpha$ -synuclein sequence  
207 that is N-terminal of the ordered core. The close packing of island A against  
208  $\beta$ 9 of the Lewy fold suggests that the corresponding interface comprises at  
209 least two consecutive small residues, which pack in the spaces between  
210 A85, S87 and A89 of  $\beta$ 9. Such residues are present in the  $\alpha$ -synuclein  
211 sequence that is N-terminal to the ordered core, e.g., G7, S9, A11, A17,  
212 A19, A27, A29, but not in the C-terminus. Although residues 14-23 of  $\alpha$ -  
213 synuclein fit into the island A density, for them to be part of the same  
214 protein chain, the (presumably disordered) connecting residues must adopt  
215 a fully extended conformation. In polymorph 2a, there is also a second  
216 substructure (residues 52-66) with similarity to the Lewy fold; it is a shorter  
217 segment than in the corresponding substructure of the recombinant  $\alpha$ -  
218 synuclein filament with phosphorylation of Y39.

219

220 Residues 47-60 of  $\alpha$ -synuclein, together with the peptide responsible for  
221 the density of island B, resemble the dimeric interface found in several  $\alpha$ -  
222 synuclein filaments formed from recombinant proteins *in vitro*, for instance  
223 polymorph 1a (PDB:6H6B) (37), overlaying residues 47-60 from one  
224 protofilament with residues 50-57 from the other, with a rmsd of 0.9 Å.  
225 The island B interface of the ordered core harbours mutations that cause  
226 inherited PD, such as G51D and A53E/G/T/V (2). Most mutations are  
227 incompatible with the interfaces of filaments assembled *in vitro*, suggesting  
228 that they are also likely to disrupt the interface with island B peptides.

229

230

### 231 Implications

232

233 We establish the existence of molecular conformers of assembled  $\alpha$ -  
234 synuclein in neurodegenerative disease (Figure 3). For tau, distinct  
235 conformers define different diseases (38). Lewy body diseases PD, PDD and  
236 DLB share the same protofilament fold, confirming that they are closely  
237 related. Dementia is common in PD, especially in advanced cases (1-3). A  
238 diagnosis of PDD is made when cognitive impairment develops in a patient  
239 with long-standing idiopathic PD, whereas dementia that develops within a  
240 year of PD is called DLB (1,4). PDD and DLB show similar neuropathological  
241 profiles, including the presence of widespread cortical  $\alpha$ -synuclein Lewy  
242 pathology (39). Many cases have also some Alzheimer-type plaques and  
243 tangles. The combination of Lewy body- and Alzheimer-type pathologies  
244 correlates well with PDD and DLB (1,40). Consistent with the presence of

245 the same protofilament in PD, PDD and DLB, Lewy pathology in the brain  
246 forms first in the brainstem, from where it progresses to limbic and cortical  
247 areas (41). These findings indicate that PD, PDD and DLB are part of a  
248 continuum of diseases. Lewy pathology is also characteristic of incidental  
249 Lewy body disease, primary autonomic failure, many cases of rapid eye  
250 movement sleep behaviour disorder and some cases of Alzheimer's disease  
251 (1,2). It remains to be seen if the  $\alpha$ -synuclein filament structures are the  
252 same as those reported here. This is also true of the Lewy pathology found  
253 in the peripheral nervous system in PD.

254

255 The filament fold of Lewy body diseases differs from that of MSA,  
256 consistent with seed amplification being able to distinguish between PD and  
257 MSA (30,42). However, known structures of seeded  $\alpha$ -synuclein aggregates  
258 are different from those of the seeds (43,44). Unlike for Lewy body  
259 diseases, two filament types have been observed in MSA, each of which is  
260 made of two different protofilaments (6). The differences between Lewy  
261 and MSA folds are consistent with differences in morphology that were  
262 described between the  $\alpha$ -synuclein filaments of DLB and MSA by negative  
263 staining (45). In the  $\alpha$ -synuclein filament structures of MSA, E46 forms a  
264 salt bridge with K80, whereas E35 forms a salt bridge with K80 in PD, PDD  
265 and DLB (Figure 3) This may explain why DLB seeds, unlike those from  
266 MSA, induced the seeded assembly of E46K  $\alpha$ -synuclein in HEK cells  
267 (31,46).

268

269 Why are the Lewy and MSA folds of  $\alpha$ -synuclein different? It will be  
270 important to know more about post-translational modifications and the  
271 identities of non-proteinaceous densities associated with these folds.  
272 Different cellular environments may play a role (23). Filaments of  
273 recombinant  $\alpha$ -synuclein, including those amplified from brain seeds, failed  
274 to adopt the same fold as filaments from human brains. To understand the  
275 mechanisms that lead to the formation of  $\alpha$ -synuclein folds, it is important  
276 to develop methods by which to assemble recombinant  $\alpha$ -synuclein into  
277 Lewy and MSA folds, similar to what has been done for Alzheimer tau  
278 filaments (47). It will also be important to identify conditions for making  
279 seeded aggregates with structures identical to those of  $\alpha$ -synuclein seeds  
280 and to produce animal models with structures of  $\alpha$ -synuclein filaments like  
281 those from human brain. Knowledge of the structures of  $\alpha$ -synuclein  
282 filaments and how they form may be used for the development of specific  
283 biomarkers for synucleinopathies and the development of safe and effective  
284 mechanism-based therapies.

285

286 **References**

287

- 288 1. Berg, D. et al. Time to redefine Parkinson's disease? Introductory  
289 statement of the MDS taskforce on the definition of Parkinson's  
290 disease. *Mov. Disord.* 29, 454-462 (2014).
- 291 2. Goedert, M., Spillantini, M.G., Del Tredici K. & Braak, H. 100 years of  
292 Lewy pathology. *Nature Rev. Neurol.* 9, 13-24 (2013).
- 293 3. Aarsland, D., Andersen K., Larsen, J.P., Lolk, A. & Kragh-Sørensen,  
294 P. Prevalence and characteristics of dementia in Parkinson disease:  
295 an 8-year prospective study. *Arch. Neurol.* 60, 387-392 (2003).
- 296 4. McKeith, I.G. et al. Diagnosis and management of dementia with  
297 Lewy bodies. Fourth consensus report of the DLB consortium.  
298 *Neurology* 879, 88-100 (2017).
- 299 5. Fanciulli, A. & Wenning, G.K. Multiple system atrophy. *N. Engl. J. Med.*  
300 372, 249-263 (2015).
- 301 6. Schweighauser, M. et al. Structures of  $\alpha$ -synuclein filaments from  
302 multiple system atrophy. *Nature* 585, 464-469 (2020).
- 303 7. Polymeropoulos, M.H. et al. Mutation in the  $\alpha$ -synuclein gene  
304 identified in families with Parkinson's disease. *Science* 276, 2045-  
305 2047 (1997).
- 306 8. Singleton, A.B. et al.  $\alpha$ -Synuclein locus triplication causes Parkinson's  
307 disease. *Science* 302, 841 (2003).
- 308 9. Zarzanz, J.J. et al. The new mutation, E46K, of alpha-synuclein  
309 causes Parkinson's disease and Lewy body dementia. *Ann. Neurol.*  
310 55, 164-173 (2004).
- 311 10. Nalls, M.A. et al. Large-scale meta-analysis of genome-wide  
312 association data identifies six new risk loci for Parkinson's disease.  
313 *Nature Genet.* 46, 989-993 (2014).
- 314 11. Davidson, W.S., Jonas, A., Clayton, D.F. & George, J.M.  
315 Stabilization of  $\alpha$ -synuclein secondary structure upon binding to  
316 synthetic membranes. *J. Biol. Chem.* 273, 9443-9449 (1998).
- 317 12. Ueda, K. et al. Molecular cloning of cDNA encoding an  
318 unrecognized component of amyloid in Alzheimer disease. *Proc. Natl.*  
319 *Acad. Sci. USA* 90, 11282-11286 (1993).
- 320 13. Li, H.T., Du, H.N., Tang, L., Hu, J. & Hu, H.Y. Structural  
321 transformation and aggregation of human  $\alpha$ -synuclein in  
322 trifluoroethanol: non-amyloid component sequence is essential and  
323  $\beta$ -sheet formation is prerequisite to aggregation. *Biopolymers* 64,  
324 221-226 (2002).

325 14. Crowther, R.A., Jakes, R., Spillantini, M.G. & Goedert, M.  
326 Synthetic filaments assembled from C-terminally truncated  $\alpha$ -  
327 synuclein. FEBS Lett. 436, 309-312 (1998).

328 15. Conway, K.A., Harper, J.D. & Lansbury P.T. Fibrils formed in  
329 vitro from  $\alpha$ -synuclein and two mutant forms linked to Parkinson's  
330 disease are typical amyloid. Biochemistry 39, 2525-2563 (2000).

331 16. Serpell, L.C., Berriman, J., Jakes, R., Goedert, M. & Crowther,  
332 R.A. Fiber diffraction of synthetic  $\alpha$ -synuclein filaments shows  
333 amyloid-like cross- $\beta$  conformation. Proc. Natl. Acad. Sci. USA 97,  
334 4897-4902 (2000).

335 17. Miake, H., Mizusawa, H., Iwatsubo, T. & Hasegawa, M.  
336 Biochemical characterization of the core structure of  $\alpha$ -synuclein  
337 filaments. J. Biol. Chem. 277, 19213-19219 (2002).

338 18. Mougenot, A.L. et al. Prion-like acceleration of a  
339 synucleinopathy in a transgenic mouse model. Neurobiol. Aging 33,  
340 2225-2228 (2012).

341 19. Luk, K.C. et al. Pathological  $\alpha$ -synuclein transmission initiates  
342 Parkinson-like neurodegeneration in nontransgenic mice. Science  
343 338, 949-953 (2012).

344 20. Masuda-Suzukake, M. et al. Prion-like spreading of pathological  
345  $\alpha$ -synuclein in brain. Brain 136, 1128-1138 (2013).

346 21. Osterberg, V.R. et al. Progressive aggregation of  $\alpha$ -synuclein  
347 and selective degeneration of Lewy inclusion-bearing neurons in a  
348 mouse model of parkinsonism. Cell Rep. 10, 1252-1260 (2015).

349 22. Peelaerts, W. et al.  $\alpha$ -Synuclein strains cause distinct  
350 synucleinopathies after local and systemic administration. Nature 522,  
351 340-344 (2015).

352 23. Peng, C. et al. Cellular milieu imparts pathological  $\alpha$ -synuclein  
353 strains in  $\alpha$ -synucleinopathies. Nature 557, 558-563 (2018).

354 24. Prusiner, S.B. et al. Evidence for  $\alpha$ -synuclein prions causing  
355 multiple system atrophy in humans with parkinsonism. Proc. Natl.  
356 Acad. Sci. USA 112, E5308-E5317 (2015).

357 25. Tarutani, A., Arai, T., Murayama, S., Hisanaga, S.I. &  
358 Hasegawa, M. Potent prion-like behaviors of pathogenic  $\alpha$ -synuclein  
359 and evaluation of inactivation methods. Acta Neuropathol. Commun.  
360 6, 29 (2018).

361 26. Yamasaki, T.R. et al. Parkinson's disease and multiple system  
362 atrophy have distinct  $\alpha$ -synuclein seed characteristics. J. Biol. Chem.  
363 294, 1045-1058 (2019).

364 27. Lavenir, I. et al. Silver staining (Campbell-Switzer) of neuronal  
365  $\alpha$ -synuclein assemblies induced by multiple system atrophy and

366 Parkinson's disease brain extracts in transgenic mice. *Acta*  
367 *Neuropathol. Commun.* 7, 148 (2019).

368 28. Klingstedt, T. et al. Luminescent conjugated oligothiophenes  
369 distinguish between  $\alpha$ -synuclein assemblies of Parkinson's disease  
370 and multiple system atrophy. *Acta Neuropathol. Commun.* 7, 193  
371 (2019).

372 29. Strohäker, T. et al. Structural heterogeneity of  $\alpha$ -synuclein  
373 fibrils amplified from patient brain extracts. *Nature Commun.* 10,  
374 5535 (2019).

375 30. Shahnawaz, M. et al. Discriminating  $\alpha$ -synuclein strains in  
376 Parkinson's disease and multiple system atrophy. *Nature* 578, 273-  
377 277 (2020).

378 31. Ayers, J.I. et al. Different  $\alpha$ -synuclein prion strains cause  
379 dementia with Lewy bodies and multiple system atrophy. *Proc. Natl.*  
380 *Acad. Sci. USA* 119, e2113489119 (2022).

381 32. Spillantini, M.G., Crowther, R.A., Jakes, R., Hasegawa, M. and  
382 Goedert, M.  $\alpha$ -Synuclein in filamentous inclusions of Lewy bodies  
383 from Parkinson's disease and dementia with Lewy bodies. *Proc. Natl.*  
384 *Acad. Sci. USA* 95, 6469-6473 (1998).

385 33. Crowther, R.A., Daniel, S.E. & Goedert, M. Characterisation of  
386 isolated  $\alpha$ -synuclein filaments from substantia nigra of Parkinson's  
387 disease brain. *Neurosci. Lett.* 292, 128-130 (2000).

388 34. Holec, S.A.M., Liu, S.L. & Woerman, A.L. Consequences of  
389 variability in  $\alpha$ -synuclein fibril structure on strain biology. *Acta*  
390 *Neuropathol.* 143, 311-330 (2022).

391 35. Zhao, K. et al. Parkinson's disease-related phosphorylation at  
392 Tyr39 rearranges  $\alpha$ -synuclein amyloid fibril structure revealed by  
393 cryo-EM. *Proc. Natl. Acad. Sci. USA* 117, 20305-20315 (2020).

394 36. McGlinchey, R.P., Ni, X., Shadish, J.A., Jiang, J. & Lee, J.C. Thje  
395 N-terminus of  $\alpha$ -synuclein dictates fibril formation. *Proc. Natl. Acad.*  
396 *Sci. USA* 118, e2023487118 (2021).

397 37. Guerrero-Ferreira, R. et al. Two new polymorphic structures of  
398 human full-length alpha-synuclein fibrils solved by cryo-electron  
399 microscopy. *eLife* 8, e48907 (2019).

400 38. Shi, Y. et al. Structure-based classification of tauopathies.  
401 *Nature* 598, 359-363 (2021).

402 39. Tsuboi, Y. & Dickson, D.W. Dementia with Lewy bodies and  
403 Parkinson's disease with dementia: Are they different? *Parkinsonism*  
404 *Relat. Disord.* 11, S47-S51 (2005).

405 40. Compta, Y. et al. Lewy- and Alzheimer-type pathologies in  
406 Parkinson's disease dementia: which is more important? *Brain* 134,  
407 1493-1505 (2011).

408 41. Braak, H. & Del Tredici K. Neuroanatomy and pathology of  
409 sporadic Parkinson's disease. *Adv. Anat. Embryol. Cell Biol.* 201, 1-  
410 119 (2009).

411 42. Poggiolini, I. et al. Diagnostic value of cerebrospinal fluid alpha-  
412 synuclein seed quantification in synucleinopathies. *Brain* 145, 584-  
413 595 (2022).

414 43. Lövestam, S. et al. Seeded assembly in vitro does not replicate  
415 the structures of  $\alpha$ -synuclein filaments from multiple system atrophy.  
416 *FEBS Open Bio* 11, 999-1013 (2021).

417 44. Burger, D., Fenyi, A., Bousset, L., Stahlberg, H. & Melki, R.  
418 Cryo-EM structure of alpha-synuclein fibrils amplified by PMCA from  
419 PD and MSA patient brains. *BioRxiv*.

420 45. Spillantini, M.G., Crowther, R.A., Jakes, R., Cairns, N.J., Lantos,  
421 P.L. & Goedert, M. Filamentous  $\alpha$ -synuclein inclusions link multiple  
422 system atrophy with Parkinson's disease and dementia with Lewy  
423 bodies. *Neurosci. Lett.* 251, 205-208 (1998).

424 46. Woerman, A.L. et al. Familial Parkinson's point mutation  
425 abolishes multiple system atrophy prion replication. *Proc. Natl. Acad.*  
426 *Sci. USA* 115, 409-414 (2018).

427 47. Lövestam, S. et al. Assembly of recombinant tau into filaments  
428 identical to those of Alzheimer's disease and chronic traumatic  
429 encephalopathy. *eLife* 11, e76494 (2022).

430

431

432

433

434

435 Acknowledgements

436

437 We thank the patients' families for donating brain tissues, T. Darling and J.  
438 Grimmett for help with high-performance computing and the EM facility of  
439 the Medical Research Council (MRC) Laboratory of Molecular Biology for  
440 help with cryo-EM data acquisition. We thank R.A. Crowther, S. Lövestam,  
441 W. Poewe, M.G. Spillantini and E. Tolosa for helpful discussions. We  
442 acknowledge Diamond Light Source for access and support of the cryo-EM  
443 facilities at the UK's Electron Bio-imaging Centre (under proposal bi23268),  
444 funded by the Wellcome Trust, the MRC and the Biotechnology and  
445 Biological Sciences Research Council (BBSRC). This work was supported by

446 the MRC (MC\_UP\_A025\_1013 to S.H.W.S. and MC\_U105184291 to M.G.).  
447 T.L. holds an Alzheimer's Research UK Senior Fellowship. T.R. is supported  
448 by the National Institute for Health Research Queen Square Biomedical  
449 Research Unit in Dementia. The Queen Square Brain Bank is supported by  
450 the Rita Lila Weston Institute for Neurological Studies. This work was also  
451 supported by the Japan Agency for Science and Technology (CREST)  
452 (JPMJCR18H3 to M.H.), the Japan Agency for Medical Research and  
453 Development (AMED) (JP20dm0207072 to M.H.), the US National Institutes  
454 of Health (P30-AG010133, U01-NS110437 and RF1-AG071177, to R.V. and  
455 B.G., and R01NS037167, to T.F.) and the Department of Pathology and  
456 Laboratory Medicine, Indiana University School of Medicine (to R.V. and  
457 B.G.).

458

459

#### 460 Author Contributions

461

462 P.W.C., Yuko Saito, T.F., T.T.W., K.H., S.M., T.R., B.G., M.H. and T.L.  
463 identified patients and performed neuropathology; Y.Y., H.J.G., R.V. and  
464 M.H. performed analysis of brain samples; Y.Y., Yang Shi, M.S., X.Z. and  
465 A.K. collected cryo-EM data; Y.Y., Yang Shi, M.S., A.G.M. and S.H.W.S.  
466 analysed cryo-EM data; Y.Y. performed immunoblot analysis; B.G., M.H.  
467 and T.L. performed immunohistochemistry; S.H.W.S. and M.G. supervised  
468 the project. All authors contributed to the writing of the manuscript.

469

470

#### 471 Competing Interests

472

473 The authors declare no competing interests.

474

475

#### 476 Additional Information

477

478 For the purpose of open access, the MRC Laboratory of Molecular Biology  
479 has applied a CC BY public copyright licence to any Author Accepted  
480 Manuscript version arising.

481

482

#### 483 Corresponding Authors

484

485 Correspondence to Sjors H.W. Scheres ([scheres@mrc-lmb.cam.ac.uk](mailto:scheres@mrc-lmb.cam.ac.uk)) and  
486 Michel Goedert ([mg@mrc-lmb.cam.ac.uk](mailto:mg@mrc-lmb.cam.ac.uk)).

487

488 Data Availability

489

490 Cryo-EM maps have been deposited in the Electron Microscopy Data Bank  
491 (EMDB) under accession number 15285. Corresponding refined atomic  
492 models have been deposited in the Protein Data Bank (PDB) under  
493 accession number 8A9L.

494

495

496

497

498

499

500

501

502

503

504

505

506

507

508

509

510

511

512

513

514

515

516

517

518

519

520

521

522

523

524

525

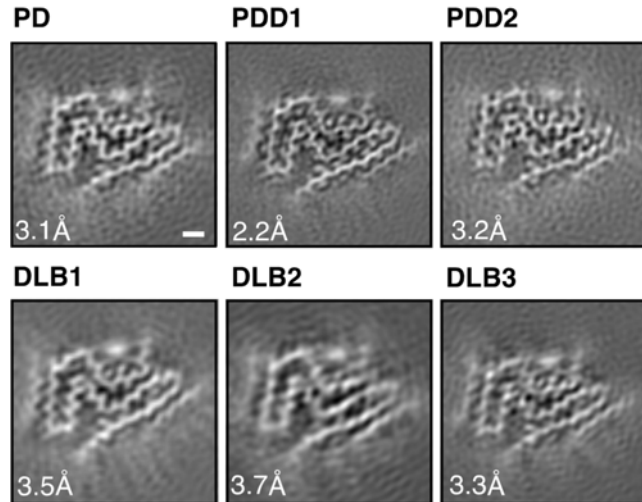
526

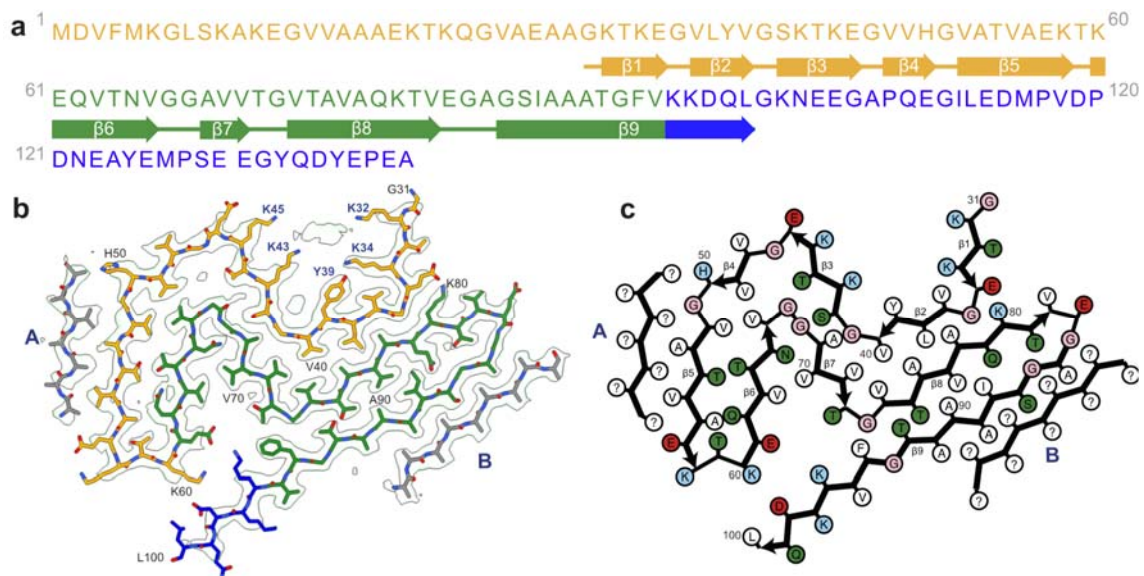
527

528

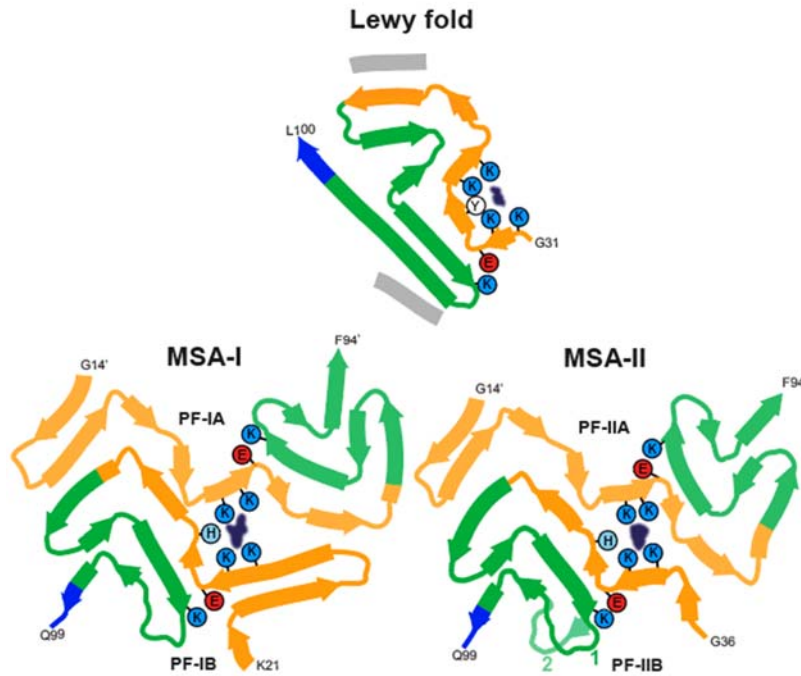
529 **FIGURES**

530





536  
537 **Figure 2. Cryo-EM structure of  $\alpha$ -synuclein filaments from Parkinson's disease, Parkinson's**  
538 **disease dementia and dementia with Lewy bodies (Lewy fold). (a).** Amino acid sequence of  
539 human  $\alpha$ -synuclein. N-terminal region (residues 1-60) in orange, NAC region (residues 61-95)  
540 in green and C-terminal region (residues 96-140) in blue. Thick connecting lines with  
541 arrowheads indicate  $\beta$ -strands. **(b).** Cryo-EM density map and atomic model of the Lewy fold.  
542 The filament core extends from G31-L100. Islands A and B are indicated in grey. **(c).** Schematic  
543 of the Lewy filament fold of  $\alpha$ -synuclein. Negatively charged residues are in red, positively  
544 charged residues in blue, polar residues in green, apolar residues in white, sulfur-containing  
545 residues in yellow and glycines in pink. Thick connecting lines with arrowheads indicate  $\beta$ -  
546 strands. Unknown residues are indicated by question marks.



547  
548

549 **Figure 3. Comparison of the Lewy and MSA  $\alpha$ -synuclein filament folds.** Schematic of  
550 secondary structure elements in the Lewy and MSA folds, depicted as a single rung, and  
551 coloured as in Figure 2 (N-terminal region of  $\alpha$ -synuclein in orange, NAC region in green and  
552 C-terminal region in blue; thick connecting lines with arrowheads indicate  $\beta$ -strands). The  
553 extra densities in all structures are depicted in dark blue. The positions of their surrounding  
554 residues, as well as the supporting salt bridges between E35 and K80 in the Lewy fold and  
555 between E46 and K80 in MSA protofilaments, are highlighted with coloured circles.

556

557 **Methods**

558

559 No statistical methods were used to predetermine sample size. The  
560 experiments were not randomized and investigators were not blinded to  
561 allocation during experiments and outcome assessment.

562

563 **Clinical history and neuropathology.** PD was in a 78-year-old woman  
564 who died with a neuropathologically confirmed diagnosis after a 22-year  
565 history of slowly progressing rest tremor and bradykinesia. PDD case 1 was  
566 in an 87-year-old man who died with a neuropathologically confirmed  
567 diagnosis following an 8-year history of prominent rest tremor and  
568 bradykinesia. He developed dementia approximately 3 years after the  
569 diagnosis of PD. This case has been described before [case 12 in (48)].  
570 PDD case 2 was in a 76-year-old woman who died with a  
571 neuropathologically confirmed diagnosis after a 13-year history of  
572 disturbed sleep, orthostatic hypotension, resting tremor and bradykinesia.  
573 She began to develop dementia approximately 4 years after the diagnosis  
574 of PD. The individuals with DLB have been described before (6). They  
575 developed dementia around the same time as PD.

576

577 **Sequencing of *SNCA* coding exons.** Genomic DNA was extracted from  
578 frozen brain tissues. Coding exons of *SNCA* and flanking intronic sequences  
579 were amplified by polymerase chain reaction and sequenced using the  
580 dideoxy method.

581

582 **Extraction of  $\alpha$ -synuclein filaments.** Sarkosyl-insoluble material was  
583 extracted from fresh-frozen cingulate cortex and frontal cortex of  
584 individuals with PD, PDD and DLB, essentially as described (25). In brief,  
585 tissues were homogenized in 20 vol (v/w) extraction buffer consisting of 10  
586 mM Tris-HCl, pH 7.5, 0.8 M NaCl, 10% sucrose and 1 mM EGTA.  
587 Homogenates were brought to 2% sarkosyl and incubated for 30 min at  
588 37° C. Following a 10 min centrifugation at 10,000g, the supernatants were  
589 spun at 100,000g for 20 min. Pellets were resuspended in 500  $\mu$ l/g  
590 extraction buffer and centrifuged at 3,000g for 5 min. Supernatants were  
591 diluted threefold in 50 mM Tris-HCl, pH 7.5, containing 0.15 M NaCl, 10%  
592 sucrose and 0.2% sarkosyl, and spun at 166,000g for 30 min. Sarkosyl-  
593 insoluble pellets were resuspended in 100  $\mu$ l/g of 20 mM Tris-HCl, pH 7.4.

594

595 **Immunolabelling and histology.** Immunogold negative-stain electron  
596 microscopy and immunoblotting were carried out as described (49).  
597 Filaments were extracted from cingulate cortex of the case of PD, PDD

598 cases 1 and 2, as well as DLB case 3. Frontal cortex was used for DLB cases  
599 1 and 2. PER4, a rabbit polyclonal serum that was raised against a peptide  
600 corresponding to residues 116-131 of human  $\alpha$ -synuclein (32), was used  
601 at 1:50. Images were acquired at 11,000x with a Gatan Orius SC200B CCD  
602 detector on a Tecnai G2 Spirit at 120 kV. For immunoblotting, samples were  
603 resolved on 4-12% Bis-Tris gels (NuPage) and primary antibodies diluted  
604 in PBS plus 0.1% Tween 20 and 5% non-fat dry milk. Before blocking,  
605 membranes were fixed with 1% paraformaldehyde for 30 min. Primary  
606 antibodies were: Syn303 [a mouse monoclonal antibody that recognizes  
607 residues 1-5 of human  $\alpha$ -synuclein (50)] (BioLegend) at 1:4,000, Syn1 [a  
608 mouse monoclonal antibody that recognizes residues 91-99 from the NAC  
609 region of human  $\alpha$ -synuclein (51)] (BD Biosciences) at 1:4,000 and PER4  
610 at 1:4,000. Histology and immunohistochemistry were carried out as  
611 described (25,52). Some sections (8  $\mu$ m) were counterstained with  
612 haematoxylin. The primary antibody was Syn1 (1:1,000).

613

614 Electron cryo-microscopy. Extracted filaments were centrifuged at 3,000  
615 g for 3 min and applied to glow-discharged holey carbon gold grids  
616 (Quantifoil Au R1.2/1.3, 300 mesh), which were glow-discharged with an  
617 Edwards (S150B) sputter coater at 30 mA for 30 s. Aliquots of 3  $\mu$ l were  
618 applied to the grids and blotted with filter paper (Whatman, cat no. 1001-  
619 070) at 100% humidity and 4°C, using a Vitrobot Mark IV (Thermo Fisher  
620 Scientific). For all cases, datasets were acquired on Titan Krios G2, G3 and  
621 G4 microscopes (Thermo Fisher Scientific) operated at 300 kV. Images for  
622 the case of PD and case 2 of PDD were acquired using a Falcon-4 detector  
623 (Thermo Fisher Scientific). Images for case 1 of PDD and case 1 of DLB  
624 were acquired using a Falcon-4i detector (Thermo Fisher Scientific) in EER  
625 mode with a flux of 8 electrons/pixel/s and a Selectris-X energy filter  
626 (Thermo Fisher Scientific) with a slit width of 10 eV to remove inelastically  
627 scattered electrons. Images for cases 1-3 of DLB were acquired with a  
628 Gatan K2 or K3 detector in super-resolution counting mode, using a Bio-  
629 quantum energy filter (Gatan) with a slit width of 20 eV. Images were  
630 recorded with a total dose of 40 electrons per  $\text{\AA}^2$ .

631

632 Helical reconstruction. Movie frames were gain-corrected, aligned, dose-  
633 weighted and then summed into a single micrograph using RELION's own  
634 motion correction program (53). Contrast transfer function (CTF)  
635 parameters were estimated using CTFFIND-4.1 (54). All subsequent image-  
636 processing steps were performed using helical reconstruction methods in  
637 RELION (55,56).  $\alpha$ -Synuclein filaments were picked manually, as they could  
638 be distinguished from filaments made of tau, A $\beta$ , and TMEM106B by their

639 general appearance (Extended Data Table 1). For all data sets,  
640 reference-free 2D classification was performed to select suitable segments  
641 for further processing. For the case of PD, PDD case 2 and DLB case 2,  
642 start-end coordinates for twisting  $\alpha$ -synuclein filaments were re-picked  
643 manually, based on individual segments that were assigned to 2D classes  
644 that corresponded to twisting filaments. Initial 3D reference models were  
645 generated *de novo* from 2D class averages using an estimated rise of 4.75  
646 Å and helical twists according to the observed cross-over distances of the  
647 filaments in the micrographs (57) for PDD case 1. The refined model from  
648 PDD case 1, low-pass filtered to 10 Å, was used as initial model for the  
649 other cases of PD, PDD and DLB. Combinations of 3D auto-refinements and  
650 3D classifications were used to select the best segments for each structure.  
651 For all data sets, Bayesian polishing (52) and CTF refinement (58) were  
652 performed to further increase the resolution of the reconstructions. Final  
653 reconstructions were sharpened using standard post-processing  
654 procedures in RELION, and overall final resolutions were estimated from  
655 Fourier shell correlations at 0.143 between the independently refined half-  
656 maps, using phase randomisation to correct for convolution effects of a  
657 generous, soft-edged solvent mask (59) (Extended Data Figure 3).  
658 Untwisted models with the Lewy fold and their projections were generated  
659 using the relion helix inimodel2d and relion project programs, respectively.  
660

661 Model building. Atomic models comprising three  $\beta$ -sheet rungs were built  
662 *de novo* in Coot (60) in the best available map for PDD case 1. Coordinate  
663 refinements were performed using *Servalcat* (61). Final models were  
664 obtained using refinement of only the asymmetric unit against the half-  
665 maps in *Servalcat*.  
666  
667  
668  
669  
670  
671  
672  
673  
674  
675  
676  
677  
678  
679

## 680 References

681

682 48. Schweighauser, M. et al. Age-dependent formation of  
683 TMEM106B amyloid filaments in human brains. *Nature* 605, 310-314  
684 (2022).

685 49. Goedert, M., Spillantini, M.G., Cairns, N.J. & Crowther, R.A. Tau  
686 proteins of Alzheimer paired helical filaments: abnormal  
687 phosphorylation of all six brain isoforms. *Neuron* 8, 159-168 (1992).

688 50. Giasson, B.I. et al. A panel of epitope-specific antibodies  
689 detects protein domains distributes throughout human  $\alpha$ -synuclein in  
690 Lewy bodies of Parkinson's disease. *J. Neurosci. Res.* 59, 528-533  
691 (2000).

692 51. Perrin, R.J. et al. Epitope mapping and specificity of the anti-  
693 alpha synuclein monoclonal antibody Syn-1 in mouse brain and  
694 cultured cell lines. *Neurosci. Lett.* 349, 133-135 (2003).

695 52. Spina, S. et al. The tauopathy associated with mutation +3 in  
696 intron 10 of *Tau*: characterization of the MSTD family. *Brain* 131, 72-  
697 89 (2008).

698 53. Zivanov, J., Nakane, T. & Scheres, S.H.W. A Bayesian approach  
699 to beam-induced motion correction in cryo-EM single particle analysis.  
700 *IUCrJ* 6, 5-17 (2019).

701 54. Rohou, A. & Grigorieff, N. CTFFIND4: fast and accurate defocus  
702 estimation from electron micrographs. *J. Struct. Biol.* 192, 216-221  
703 (2015).

704 55. He, S. & Scheres, S.H.W. Helical reconstruction in RELION. *J.*  
705 *Struct. Biol.* 198, 163-176 (2017).

706 56. Zivanov, J. et al. New tools for automated high-resolution cryo-  
707 EM structure determination in RELION-3. *eLife* 7, e42166 (2018).

708 57. Scheres, S.H.W. Amyloid structure determination in RELION-  
709 3.1. *Acta Crystallogr. D* 76, 94-101 (2020).

710 58. Zivanov, J., Nakane T. & Scheres, S.H.W. Estimation of higher-  
711 order aberrations and anisotropic magnification from cryo-EM data  
712 sets in RELION-3.1. *IUCrJ* 7, 253-267 (2020).

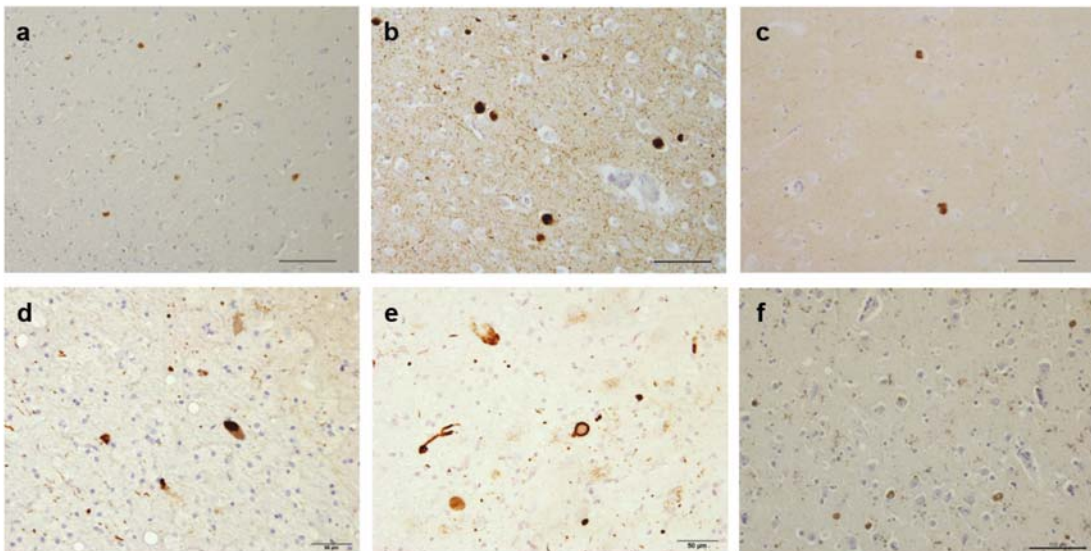
713 59. Chen, V.B. et al. MolProbity: all-atom structure validation for  
714 macromolecular crystallography. *Acta Crystallogr. D* 66, 12-21  
715 (2010).

716 60. Casañal, A. et al. Current developments in Coot for  
717 macromolecular model building of electron cryo-microscopy and  
718 crystallographic data. *Protein Sci.* 29, 1069-1078 (2020).

719 61. Yamashita, K., Palmer, C.M., Burnley, T. & Murshudov, G.N.  
720 Cryo-EM single-particle structure refinement and map calculation  
721 using *Servalcat*. *Acta Crystallogr. D* 77, 1282-1291 (2021).  
722

723 **EXTENDED DATA FIGURES**

724

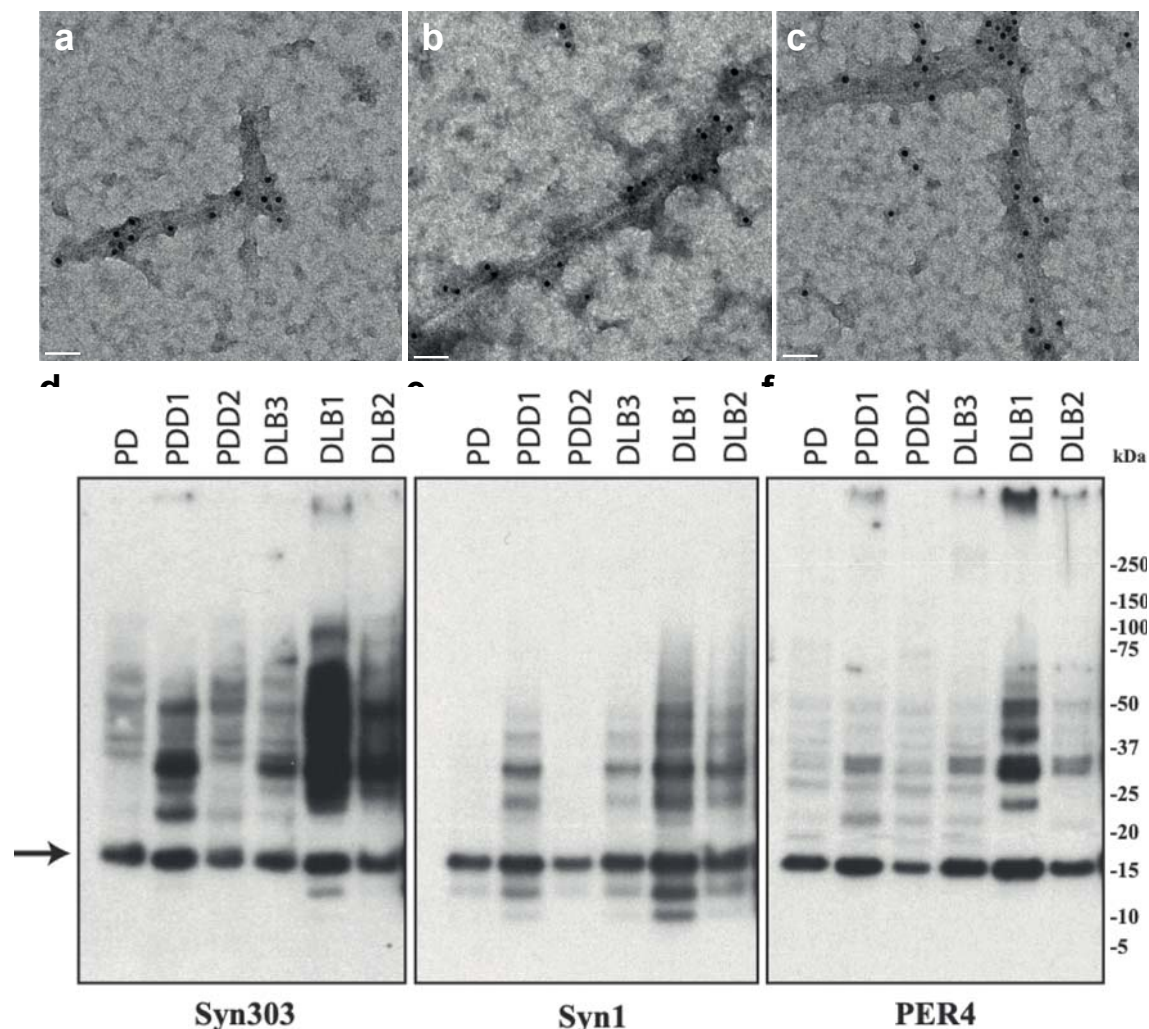


725

726

727 **Extended Data Figure 1. Immunostaining of  $\alpha$ -synuclein inclusions.** Sections from brain  
728 regions contralateral to those used for cryo-EM structure determination were stained with  
729 monoclonal antibody Syn1 (1:1,000). (a), Cingulate cortex from PD; (b), Cingulate cortex from  
730 PDD1; (c), Cingulate cortex from PDD2; (d), Frontal cortex from DLB1; (e), Frontal cortex from  
731 DLB2; (f), Cingulate cortex from DLB3. Scale bars: a-c, f, 100  $\mu$ m; d,e, 50  $\mu$ m.

732

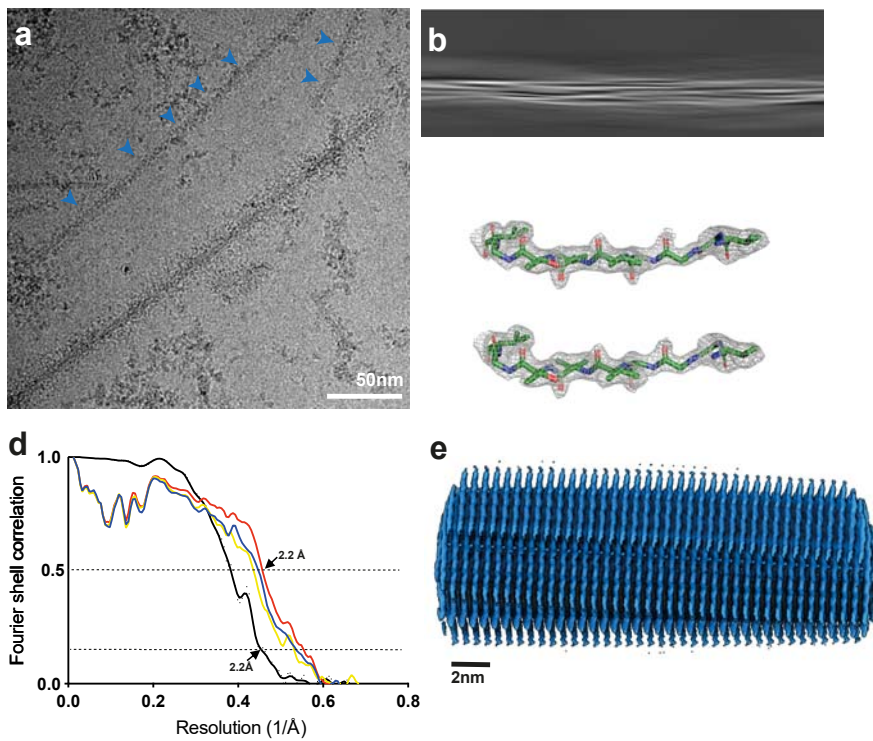


733

734

735 **Extended Data Figure 2. Negative-stain immunoelectron microscopy and**  
736 **immunoblotting of sarkosyl-insoluble material.** PER4 was used at 1:50 in (a-c). (a), PD  
737 (Cingulate cortex); (b), PDD1 (Cingulate cortex); (c), DLB3 (Cingulate cortex); Syn303, Syn1  
738 and PER4 were used at 1:4,000 in (d-f). The brain regions used for cryo-EM were also used  
739 for immunoblotting. The arrow points to the position of monomeric α-synuclein.

740

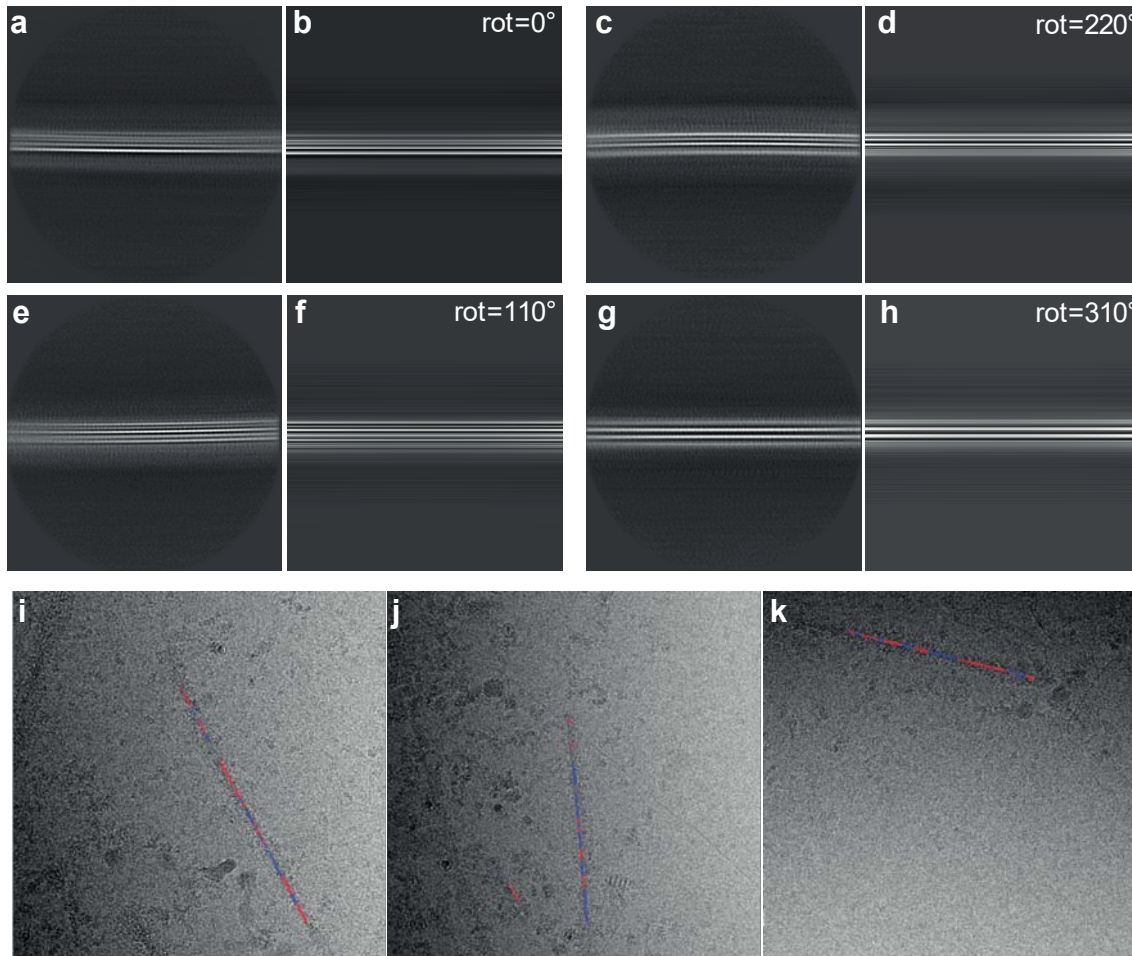


741

742

743 **Extended Data Figure 3. Cryo-EM maps, cryo-EM images and resolution estimates.** (a),  
744 alpha-Synuclein filaments (blue arrows) from PDD1. Scale bars, 50 nm. (b), Projection features of  
745 Lewy filament. Scale bars, 5 nm. (c), Zoomed-in view of the main chain showing density of the  
746 oxygen atoms. (d), Fourier shell correlation (FSC) curves for cryo-EM maps are shown in  
747 black; for the final refined atomic model against the final cryo-EM map in red; for the atomic  
748 model refined in the first half map against that half map in blue; for the refined atomic model  
749 in the first half map against the other half map in yellow. (e), Side view of the Lewy fold.

750

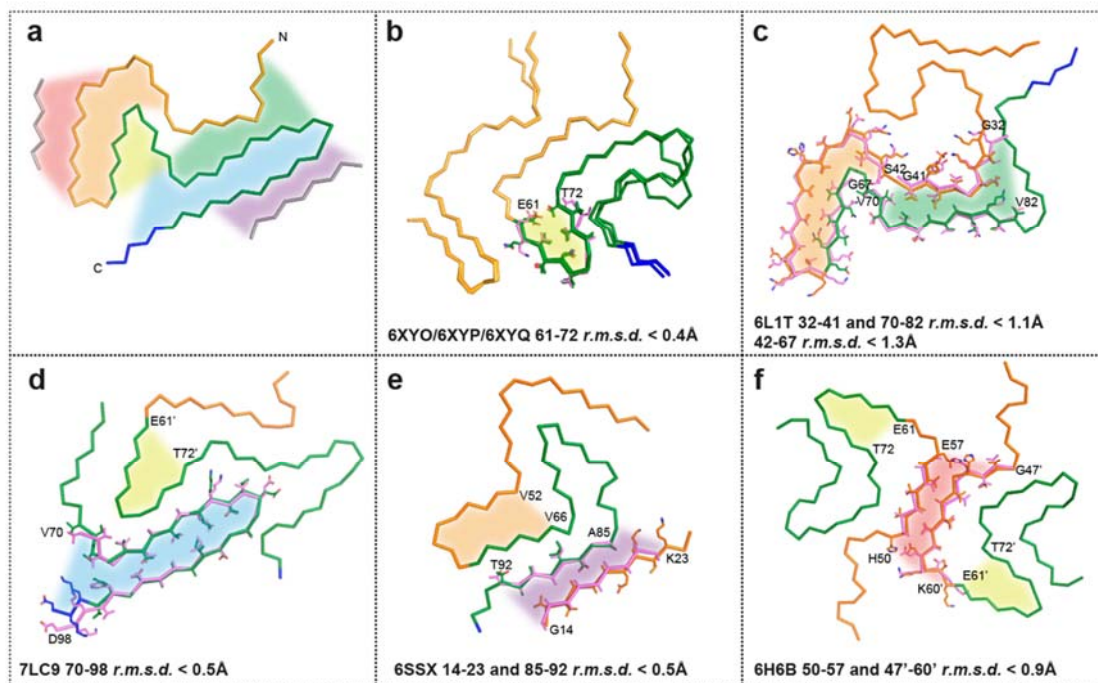


751

752

753 **Extended Data Figure 4. Twisted and untwisted filaments in 2D class averages and**  
754 **micrographs.** Case 1 of PDD was used. (a,c,e,g), 2D class averages of untwisted filaments;  
755 (b,d,f,h) projections of untwisted models with the Lewy fold, rotated by 0, 220, 110 and 310  
756 degrees, respectively, along the first Euler angle (rot). Box size, 640 Å. (i,j,k), Micrographs of  
757 untwisted and twisted filaments. Blue indicates segments that contributed to twisted 2D class  
758 averages and red segments that contributed to untwisted 2D class averages.

759



760  
761

**Extended Data Figure 5. Comparison of the Lewy fold with structures of  $\alpha$ -synuclein filaments from human brains or assembled from recombinant proteins.** (a), Ribbon plot of the Lewy fold; the protein chain is coloured as in Figure 2. Highlighted by red, orange, yellow, green, blue and purple areas are substructures that are individually shared with other filament structures. These local similarities are indicated with the same coloured areas and the overlays of the corresponding substructures are shown in sticks on the following panels (b-f). (b), Common core structure of MSA Type I and Type II filaments (made of PFIA/IIA 14-47 and PFIB/IIB 41-99), with a shared substructure highlighted in yellow. (c), pY39  $\alpha$ -synuclein protofilament (PDB:6L1T) with two different substructures highlighted in orange and green. (d), N-terminally truncated  $\alpha$ -synuclein (40-140) dimeric filament (PDB:7LC9), with two different substructures in its protofilaments, highlighted in blue and yellow. (e), Polymorph 2a filament (PDB:6SSX), with two substructures highlighted in purple and orange. (f), Polymorph 1a filament (PDB:6H6B) contains yellow-coloured substructures in its protofilaments and a red-coloured substructure in their dimeric interface.

776  
777

778 **EXTENDED DATA TABLES**

779

780 **Extended Data Table 1. Filament types.**

781

| Case | Disease | Age (yrs) | $\alpha$ -Synuclein | Tau | A $\beta$ 42 | TMEM106B |
|------|---------|-----------|---------------------|-----|--------------|----------|
| 1    | PD      | 78        | 55%                 | <1% | 10%          | 35%      |
| 2    | PDD1    | 87        | 42%                 | 38% | 5%           | 15%      |
| 3    | PDD2    | 76        | 58%                 | <1% | 5%           | 37%      |
| 4    | DLB1    | 59        | 60%                 | 10% | 27%          | 3%       |
| 5    | DLB2    | 74        | 59%                 | <1% | 5%           | 36%      |
| 6    | DLB3    | 78        | 54%                 | 12% | 22%          | 12%      |

782

783 **Extended Data Table 2. Cryo-EM data acquisition and structure determination.**

784

---

**PDD1**  
(EMD-15285, PDB 8A9L)

---

**Data acquisition**

|   |            |
|---|------------|
| Electron gun                                    | CFEG       |
| Detector  | Falcon 4i  |
| Energy filter slit (eV)                         | 10         |
| Magnification                                   | 165,000    |
| Voltage (kV)                                    | 300        |
| Electron dose (e <sup>-</sup> /Å <sup>2</sup> ) | 40         |
| Defocus range (μm)                              | 0.6 to 1.4 |
| Pixel size (Å)                                  | 0.727      |

**Map refinement**

|                               |        |
|-------------------------------|--------|
| Symmetry imposed              | C1     |
| Initial particle images (no.) | 566649 |
| Final particle images (no.)   | 68330  |
| Map resolution (Å)            | 2.2    |
| FSC threshold                 | 0.143  |
| Helical twist (°)             | 0.86   |
| Helical rise (Å)              | 4.76   |

**Model refinement**

|  |        |
|--|--------|
| Model resolution (Å)                             | 2.2    |
| FSC threshold                                    | 0.5    |
| Map sharpening <i>B</i> factor (Å <sup>2</sup> ) | -35    |
| Model composition                                |        |
| Non-hydrogen atoms                               | 2880   |
| Protein residues                                 | 430    |
| Ligands  | 0      |
| <i>B</i> factors (Å <sup>2</sup> )               |        |
| Protein  | 44.5   |
| R.m.s. deviations                                |        |
| Bond lengths (Å)                                 | 0.0063 |
| Bond angles (°)                                  | 1.16   |

Validation

|                   |       |
|-------------------|-------|
| MolProbit score   | 1.6   |
| Clashscore        | 6.34  |
| Poor rotamers (%) | 0     |
| Ramachandran plot |       |
| Favored (%)       | 96.25 |
| Allowed (%)       | 3.75  |
| Disallowed (%)    | 0     |

785

786